# Near Field Modeling for THz Wireless Channel in Nettop Size Metal Enclosures

Jinbang Fu, Prateek Juyal, and Alenka Zajić *Senior Member, IEEE* Georgia Institute of Technology, Atlanta, GA 30332 USA

Abstract—This paper proposes a path loss model and a geometry-based statistical model for Terahertz (THz) chip-to-chip wireless communication in nettop size metal enclosures. The proposed path loss model captures the attenuation of traveling wave and the gain of the electromagnetic horn in near-field region, also the resonant modes in the metal enclosure. The proposed geometric channel model describes the propagation of the traveling wave and the wave generated from the excited walls as a superposition of line of sight (LoS) and multi-bounced (MB) rays. Measurements for LoS propagation in near-field region have been performed in the indoor environment and in a nettop size empty metal enclosure. A good agreement between the measured and model predicted results has been observed, which proves the validity of the proposed models.

*Index Terms*—path loss model, THz communications, propagation, measurements.

#### I. INTRODUCTION

With the development of cellular and wireless local area network, wireless communication is now gradually replacing the wired communication with the advantage of mobility, simplicity, and convenience. The ever-growing channel capacity of wireless communication systems permits it to be a future solution for the chip-to-chip communication inside the computing device. To catch the data rate of wired systems, THz frequency is preferred for its larger available bandwidth and requiring smaller antenna size and spacings, which makes it possible to integrate more antennas to provide additional links. THz wireless channel characterization and modeling in practical scenarios are required to design such a chip-tochip wireless communication system. On-board THz wireless communication channel measurements has been performed in [1]. Also, characterization of waveguide like structures with different dimensions at 60 and 300 GHz has been conducted in [2]. Furthermore, measurements have been done inside a rectangular metal enclosure which resembles the practical desktop. It found that both traveling wave and resonant modes exist inside the metal cavity. Based on this finding, a path loss model which consists of the traveling loss, resonant modes-based power variation, and the loss due to the radiation pattern of the directional antennas has been proposed in [3], and a statistical channel model which can be considered as the superposition of LoS, single bounce double bounce, and multiple bounce rays has been proposed in [4].

This work has been supported, in part, by NSF grant 1651273. The views and findings in this paper are those of the authors and do not necessarily reflect the views of NSF.

As a step towards a thin client based always online computer, many companies has published their nettop (mini PC) with smaller size and low power consumption. Considering the size of most nettops in the market, the possible intra-chip wireless communications in such devices would be always in the near-field region of the antennas. For this practical scenario and as an extension of our previous works, this paper proposed a path loss model and a geometry based statistical channel model based on the propagation mechanisms of THz signal in a nettop size metal enclosure. The proposed path loss model accounts the attenuation of the traveling wave in near-field with the consideration of the correction ratio for the gain of horn antenna in near-field. Also, the resonant modes based power variation and the loss due to radiation pattern of the antenna used are considered too. The geometric channel model was derived based on the cavity environment and the statistical properties of the channel. The proposed channel model focuses on the traveling wave and the generated wave from the excited walls and models the channel as the superposition of the LoS and MB rays. To verify the validity of proposed models, measurements have been conducted. The measured results match well with the model predictions.

The remainder of the paper is organized as follows. Section II proposes the path loss model that captures the performance of traveling in the near-field region. Section III provides the geometry based parametric statistical channel model which describes the propagation mechanisms in an empty metal cavity. Section IV verifies the correctness of the proposed path loss and statistical channel model by comparing the simulated and measured results. Section V draw a concluding remarks.

#### II. PATH LOSS MODEL

This section introduces a near-field path loss model to approximate the THz propagation loss inside a small metal cavity. In our previously proposed resonance based THz propagation loss model, the path loss inside a desktop size metal cavity is depicted by the traveling loss, resonant modes based power variation, and the loss due to the radiation pattern of the directional antennas used in the model and the measurements. Similarly, for the near-field THz wireless channel inside a small metal enclosure, the path loss  $(PL_{dB})$  can also be estimated with these three terms and expressed as

$$(PL)_{dB} = \overline{(PL)_{dB}^{t}} + 10log_{10}(|E|^{2})^{-1} + 10log_{10}([g(\alpha_{t})g(\alpha_{r})]^{2})^{-1} + X_{\sigma}.$$
(1)

The term  $\overline{(PL)_{dB}^t}$  is the mean path loss of traveling wave. In [3], it is calculated by averaging the Friis formula over

the available bandwidth of the channel. However, in the near field region, Friis formula may not be applicable to describe the propagation loss. Based on the behaviors of electric and magnetic field signals in the near field region, the path loss models in near field were proposed in [5] and can be expressed as

$$(PL)_E^t = 4\left(\frac{1}{(kd)^2} - \frac{1}{(kd)^4} + \frac{1}{(kd)^6}\right)^{-1},\tag{2}$$

$$(PL)_H^t = 4\left(\frac{1}{(kd)^2} + \frac{1}{(kd)^4}\right)^{-1},$$
 (3)

where  $k = 2\pi/\lambda = 2\pi f/c_0$  is the wave number and d is the distance between transceivers.

Directional horns are preferred mostly for THz wireless communication to compensate the high propagation loss. The absolute gain of a standard horn is usually measured by determining the propagation loss with respect to the distance between two identical horns. However, the far-zone transmission formula may not hold for the near-field region. Hence correction ratios are required. The correction ratio for pyramid horn was derived and generalized in [6]. But for diagonal horn which was used in our measurements, correction ratio is not available and hence we present the derivation of correction ratio using the method presented in [6]. In far-field region, the power transmission can be determined by the well known Friis formula  $\frac{P_R}{P_T}=(\frac{G\lambda}{4\pi r})^2$  from which the gain can be derived as

$$G = \frac{4\pi r}{\lambda} (P_R/P_T)^{1/2}. \tag{4}$$

However, when the distance between horns is relative short, this formula may introduce considerable errors. Using the Lorentz reciprocity theorem [6], it is shown that when the tangential components of E and H are related by free space impedance, the power transmission formula between two antennas for any separation is

Impedance, the power transmission formula between two antennas for any separation is
$$\frac{P_R}{P_T} = \frac{\left| \int_{S_1} E_1^t(p) \frac{e^{-jkr}}{r} \int_{S_2} E_2^t(P') dS_1 dS_2 \right|^2}{\lambda^2 \int_{S_1} |E_1^t(P)|^2 dS_1 \int_{S_2} |E_2^t(P')|^2 dS_2}, \tag{5}$$

where  $E_1$  and  $E_2$  are the E-field transmitted by antenna 1 and antenna 2, respectively, and P, P' are the points on the aperture surfaces  $S_1$  and  $S_2$ , respectively. The tangential E-field equations at the aperture of diagonal horn are given in [7] as

$$E_1^t \approx E_1^\beta = \frac{E_0}{\sqrt{2}} \left( \cos \frac{\pi y}{2a} + \cos \frac{\pi x}{2a} \right) e^{jk \left[ \frac{2a^2 - x^2 - y^2}{2L} \right]},$$
 (6)

$$E_2^t \approx E_2^\beta = \frac{E_0}{\sqrt{2}} \left( \cos \frac{\pi \eta}{2a} + \cos \frac{\pi \zeta}{2a} \right) e^{jk \left[ \frac{2a^2 - \zeta^2 - \eta^2}{2L} \right]}. \tag{7}$$

Please note that, only the co-polarized field ( $\beta$  directed) is considered here to reduce the complexity. The geometry of the diagonal horn is shown in Fig.1. For the horns used in our measurements, L=2 cm and 2a=4.2 mm. The

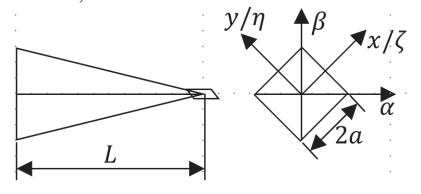


Fig. 1. The geometry of the diagonal horn.

distance between P and P' on then aperture surfaces can be approximated as  $r\approx d+[(x-\zeta)^2+(y-\eta)^2]/(2d)$ .

By taking equations (6), (7) into (5) and (4), The near field and far field gains can be derived as

$$G_{N} = \frac{2\pi r E_{0}^{2} \left| \int_{S_{1}} \int_{S_{2}} (\cos\frac{\pi y}{2a} + \cos\frac{\pi x}{2a}) (\cos\frac{\pi \eta}{2a} + \cos\frac{\pi \zeta}{2a}) \right|}{\lambda^{2} \int_{S_{1}} (\cos\frac{\pi y}{2a} + \cos\frac{\pi x}{2a})^{2} dS_{1}} \cdot \left| e^{-jk \left( \frac{x^{2} + \zeta^{2} + y^{2} + \eta^{2}}{2L} + \frac{(x - \zeta)^{2} + (y - \eta)^{2}}{2d} \right)} dS_{1} dS_{2} \right|,$$
(8)
$$G = \frac{2\pi r E_{0}^{2} \left| \int_{S_{1}} \int_{S_{2}} (\cos\frac{\pi y}{2a} + \cos\frac{\pi x}{2a}) (\cos\frac{\pi \eta}{2a} + \cos\frac{\pi \zeta}{2a}) \right|}{\lambda^{2} \int_{S_{1}} (\cos\frac{\pi y}{2a} + \cos\frac{\pi x}{2a})^{2} dS_{1}} \cdot \left| e^{-jk \left( \frac{(x - \zeta)^{2} + (y - \eta)^{2}}{2d} \right)} dS_{1} dS_{2} \right|.$$
(9)

The correction ratio is given by taking the ratio of equation (8) and (9) as

$$C_{horn} = G/G_{N}$$

$$= \frac{\left| \int_{-a}^{a} \int_{-a}^{a} \int_{-a}^{a} \int_{-a}^{a} (\cos \frac{\pi y}{2a} + \cos \frac{\pi x}{2a}) (\cos \frac{\pi \eta}{2a} + \cos \frac{\pi \zeta}{2a}) \right|}{\left| \int_{-a}^{a} \int_{-a}^{a} \int_{-a}^{a} \int_{-a}^{a} (\cos \frac{\pi y}{2a} + \cos \frac{\pi x}{2a}) (\cos \frac{\pi \eta}{2a} + \cos \frac{\pi \zeta}{2a}) \right|} \times \frac{\left| e^{-jk \left( \frac{x^{2} + \zeta^{2} + y^{2} + \eta^{2}}{2L} + \frac{(x - \zeta)^{2} + (y - \eta)^{2}}{2d} \right)} dx d\zeta dy d\eta \right|}{\left| e^{-jk \left( \frac{(x - \zeta)^{2} + (y - \eta)^{2}}{2d} \right)} dx d\zeta dy d\eta \right|}.$$
 (10)

The overall path loss of traveling wave in near-field region,  $\overline{(PL)^t}$ , can be calculated by averaging the combination of equation (2) and (10) over the available bandwidth of the channel as

$$\overline{(PL)^t} = \int_{\Delta f} C_{horn} \cdot 4 \left( \frac{1}{(kd)^2} - \frac{1}{(kd)^4} + \frac{1}{(kd)^6} \right)^{-1} df. \quad (11)$$

Please note that equation (11) calculates the path loss for electric field, and the path loss for the magnetic field signal can be calculated by averaging the combination of equation (3) and (10) over the bandwidth. In the radiating near-field, the difference between the path loss calculated from the electric and magnetic field is very small. Hence, we choose equation (11) to calculate the path loss of traveling wave in near-field.

The term  $10log_{10}(|E|^2)^{-1}$  represents the received power variation due to the resonant modes inside the metal cavity and the term  $10log_{10}([g(\alpha_t)g(\alpha_r)]^2)^{-1}$  describes the loss due to the misalignment between the Tx and Rx. Parameters  $\alpha_t$  and  $\alpha_r$  represent the angle of departure (AoD) and the angle of arrival (AoA), respectively. The parameter  $g(\alpha)$  is the radiation pattern of the antenna. The derivation of these two terms can be found in [3]. The difference between the predicted and actual path loss is captured by  $X_\sigma$ , which can be modeled as a zero-mean Gaussian random variable with standard deviation  $\sigma$ . It describes the random shadowing effects.

#### III. GEOMETRY BASED STATISTICAL CHANNEL MODEL

This section introduces a geometrical model for the short-distance LoS propagation in a small metal cavity. It is found in [8] that both traveling wave and resonant modes exist inside the metal cavity. Also, the traveling wave bounces back and forth between the sidewalls where the transceivers are positioned. To capture the propagation mechanism, we introduce an integrated geometrical model which describes the propagation as a superposition of LoS and multi-bounced (MB) rays.

Figure 2 illustrates the propagation mechanisms inside the metal cavity whose length and height are denoted by L and  $h_c$ . Antennas of Tx and Rx are assumed to be positioned on the opposite sidewalls of the metal cavity and are represented by  $A_t$  and  $A_r$ , respectively. The height and half-beamwidth of  $A_t$  and  $A_r$  are denoted as  $h_t$ ,  $\theta_t$  and  $h_r$ ,  $\theta_r$ , respectively. The angle of departure and the angle of arrival for LoS propagation are denoted as  $\alpha_t^{LoS}$  and  $\alpha_r^{LoS}$  which can be calculated as

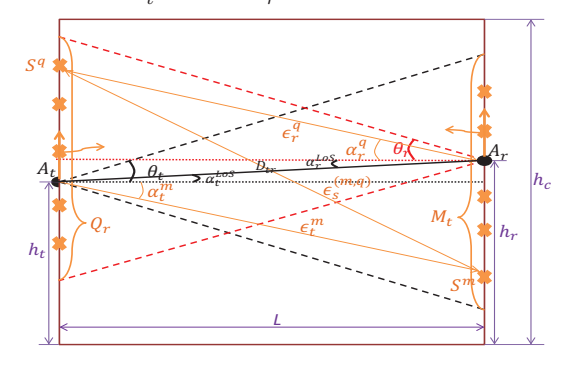


Fig. 2. The geometrical model for short distance LoS propagation in a small metal\_enclosure.

The analysis of  $\alpha_t^{LoS} = \arctan(\frac{h_r - h_t}{L})$  and  $\alpha_r^{LoS} = \arctan(\frac{h_t - h_r}{L})$ . The angles  $\alpha_t^{LoS}$  and  $\alpha_r^{LoS}$  are limited by the beamwidths of  $A_t$  and  $A_r$ , which means  $-\theta_t \leq \alpha_t^{LoS} \leq \theta_t$  and  $-\theta_r \leq \alpha_r^{LoS} \leq \theta_r$ . The distance between  $A_t$  and  $A_r$  is denoted by  $D_{tr}$  which can be calculated as  $D_{tr} = \sqrt{L^2 + (h_t - h_r)^2}$ . Different with the propagation in free space, the metal cavity is excited by the traveling wave inside, which means that the sidewalls where transceivers are positioned on can be treated both as consecutive scatters and the sources of EM waves. The LoS propagation of generated EM waves are modeled as multibounced (MB) rays for which the signals periodically bounce back and forth between the transceiver sidewalls. As shown in Fig.2, it is assumed that the sidewall with  $A_r$  consists of  $M_t$ scatters seen by the Tx, and  $Q_r$  scatters seen by the Rx on the opposite sidewall. The  $m^{th}$  and  $q^{th}$  scatter on the Rx and Tx sidewall are denoted as  $S^m$  and  $S^q$ , respectively, where  $1 \leq m \leq M_t$  and  $1 \leq q \leq Q_r$ . The distance of  $A_t \to S^m$ ,  $S_m o S^q$ , and  $S_q o A_r$  are denoted as  $\epsilon_t^m$ ,  $\epsilon_s^{m,q}$ , and  $\epsilon_r^q$ , respectively. The angle  $\alpha_t^m$  represents the angle of departure for the ray that hits the scatter  $S^m$ , and the angle  $\alpha_r^q$  represents the angle of arrival for the ray that reflects from the scatter  $S^q$ . Both  $\alpha_t^m$  and  $\alpha_r^q$  are limited by the beamwidths of  $A_t$ and  $A_r$ . With angles  $\alpha_t^m$  and  $\alpha_r^q$ , the distances  $\epsilon_t^m$ ,  $\epsilon_s^{m,q}$ , and  $\epsilon_r^q$  can be calculated as  $\epsilon_t^m = L/\alpha_t^m$ ,  $\epsilon_r^q = L/\alpha_r^q$ , and  $\epsilon_s^{(m,q)} = \sqrt{(L\tan(\alpha_t^m) - L\tan(\alpha_r^q) + h_t - h_r)^2 + L^2}$ . From the geometrical model, the time-invariant input delay

spread function of the THz wireless link can be expressed as the superposition of LoS and MB rays as

$$h(\tau) = h_{LoS}(\tau) + h_{MB}(\tau), \tag{12}$$

$$h_{LoS}(\tau) = \sqrt{\frac{K}{K+1}} A_{LoS} e^{j\phi_{LoS}} \delta(\tau - \tau_{LoS}), \tag{13}$$

$$h_{MB}(\tau) = \sqrt{\frac{1}{K+1}} \lim_{M_t, Q_r} \frac{1}{\sqrt{M_t Q_r}} \sum_{n=1}^{N} \sum_{m=1}^{M_t} \sum_{q=1}^{Q_r}$$

$$\sqrt{k_n} A_{MB}^{(n,m,q)} e^{j\phi_{MB}^{(n,m,q)}} \delta(\tau - \tau_{MB}^{(n,m,q)}),$$
 (14)

where K is the Ricean factor. The phase delay of LoS and MB rays are represented by  $\phi_{LoS}$  and  $\phi_{MB}^{(n,m,q)}$ .  $A_{LoS}$  and  $A_{MB}^{(n,m,q)}$  are the amplitudes of the LoS and multi-bounced component and can be calculated as  $A_{LoS} = \sqrt{(P_t G_t G_r)/PL_{LoS}}$ ,  $A_{MB}^{(n,m,q)} = \sqrt{(P_t G_t G_r)/PL_{MB}^{(n,m,q)}}$ , where  $P_t$ ,  $G_t$ ,  $G_r$ ,  $PL_{LoS}$ , and  $PL_{MB}^{(n,m,q)}$  are the transmit power, Tx antenna gain, Rx antenna gain, LoS path loss, and the path loss of MB rays, respectively. The path loss  $PL_{LoS}$  can be calculated by following the steps presented in SectionII with the signal traveled distance  $d=D_{tr}$ . And the signal traveled distance for MB rays is  $D_{MB}=\epsilon_t^m+\epsilon_r^q+(2n-1)\epsilon_{avg}$ , where 2n-1 represents the number of times that the signal bouncing back and forth between the transceiver sidewalls and  $\epsilon_{avq}$  is the average of the distances between the scatters on the Rx sidewall and Tx sidewall and can be calculated as  $\epsilon_{avg}$  =  $\frac{1}{M_tQ_r}\sum_{m=1}^{M_t}\sum_{q=1}^{Q_r}\epsilon_s^{(m,q)}$ . The distance  $D_{MB}$  is always in the far-field region of the horn. Hence, different with  $PL_{LoS}$ , the calculation of  $PL_{MB}$  should follow the procedures of the path loss calculation in far-field region which can be found in [3]. The time-invariant transfer function can be derived by taking the Fourier transform of the input delay-spread function

$$T(f) = \mathcal{F}_{\tau}\{h(\tau)\} = T_{LoS}(f) + T_{MB}(f), \tag{15}$$

$$T_{LoS}(f) = \sqrt{\frac{K}{K+1}} A_{LoS} e^{j\phi_{LoS} - j2\pi f \tau_{LoS}},$$
 (16)

$$T_{MB}(f) = \sqrt{\frac{1}{K+1}} \lim_{M_t, Q_r} \frac{1}{\sqrt{M_t Q_r}} \sum_{n=1}^{N} \sum_{m=1}^{M_t} \sum_{q=1}^{Q_r} \sqrt{k_n} A_{MB}^{(n,m,q)} e^{j\phi_{MB}^{(n,m,q)} - j2\pi f \tau_{MB}^{(n,m,q)}}.$$
 (17)

The transfer function  $T_{MB}$  is a Gaussian random process which is independent with  $T_{LoS}$ . Therefore, the normalized auto-correlation function of T(f) can be derived as

$$R(\Delta f) = \frac{E[T(f)^*T(f + \Delta f)]}{\sqrt{Var[T(f)]Var[T(f)]}} = R_{LoS}(\Delta f) + R_{MB}(\Delta f),$$
(18)

$$R_{LoS}(\Delta f) = \frac{E[T_{LoS}(f)^* T_{LoS}(f + \Delta f)]}{\Omega},$$

$$R_{MB}(\Delta f) = \frac{E[T_{MB}(f)^* T_{MB}(f + \Delta f)]}{\Omega},$$
(20)

$$R_{MB}(\Delta f) = \frac{E[T_{MB}(f)^* T_{MB}(f + \Delta f)]}{\Omega},$$
(20)

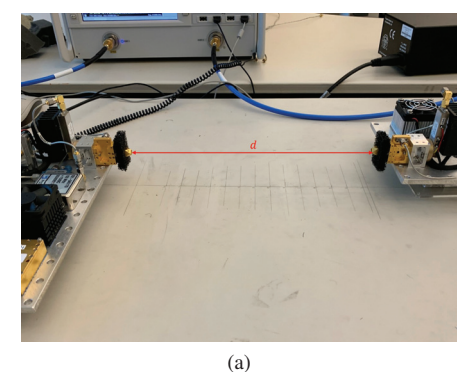
where  $(.)^*$  represents the complex conjugate, E[.] is the statistical expectation operator, Var[.] represents the statistical variance operator, and  $\Omega = P_tG_tG_r/PL_{LoS}$ . Since the number of scatters defined in the geometrical model is close to infinity, the angles  $\alpha_t^m$  and  $\alpha_r^q$  can be replaced with the independent uniform distributed random variables  $\alpha_t$  and  $\alpha_r$ whose probability density functions (pdf) are  $f(\alpha_t) = \frac{1}{2\theta_t}$ , and  $f(\alpha_r) = \frac{1}{2\theta_r}$ . Therefore, the auto-correlation functions of LoS and MB rays can be calculated as

$$R_{LoS} = \frac{K}{K+1} e^{\frac{-j2\pi\Delta f D_{tr}}{c_0}},$$
(21)

$$R_{MB} = \frac{1}{K+1} \sum_{n=1}^{N} k_n \int_{-\theta_t}^{\theta_t} \int_{-\theta_r}^{\theta_r} \frac{PL_{LoS}}{PL_{MB}} e^{-j2\pi\Delta f \tau_{MB}} d\alpha_r d\alpha_t.$$
(22)

### IV. MEASUREMENTS AND MODEL VERIFICATION

To verify the proposed path loss and PDP model, we performed measurements and compared the results with the simulations in this section. The near-field is limited by the Fraunhofer distance which can be calculated as  $d_F=2D^2/\lambda$ , where D is the largest dimension of the radiator. For the horn used in our THz measurements, the physically measured D is about 9 mm, which means that the near-field region is limited to 16 cm. The first measurement is the indoor LoS propagation with the distance between transceivers ranging from 4 cm to 16 cm with the step size of 2 cm as shown in Fig. 3a. The measured path loss is compared with the near-field path loss model (equation (11)) prediction shown in Fig. 3b. As shown in the plot, the measured path loss generally matches well with the model prediction and the biggest difference at  $d=4\mathrm{cm}$  is even less than 1 dB, which proves the validity of our derived path loss model for the traveling wave in radiating near-field region



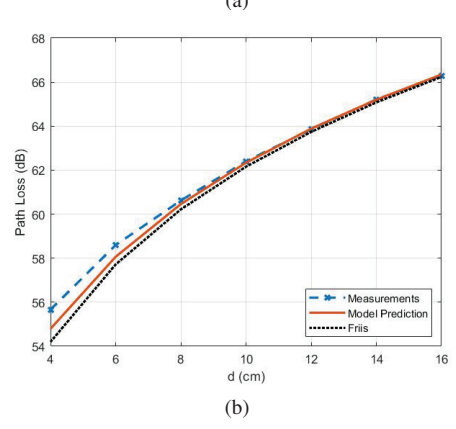


Fig. 3. (a) Measurements setup, (b) Comparison of the measured, model predicted, and Friis calculated near-field propagation loss for traveling wave in the indoor environment with respect to d.

The second measurement was performed in a Intel-mini size metal cavity with LoS propagation being considered. In this measurement, an aluminum cavity was fabricated with the size of  $11 \text{ cm} \times 11 \text{ cm} \times 5 \text{ cm}$ , which is close to the size of Intel-mini PC [9]. As shown in Fig. 4a, the fabricated metal cavity was put in between the Tx and Rx with antennas aligned horizontally. Based on the heights of antennas, two diagonal openings with the horn size were drilled on the transceiver sidewalls of the metal cavity. Hence, the distance between two transceivers was fixed by the length of the metal cavity (11 cm) which falls into the near-field region of the horn. To characterize the resonant modes in the metal enclosure, measurements were performed by varying the heights of transceivers  $h_t$  and  $h_r$ , simultaneously from 0.3075 cm to 2.4075 cm with the step size of 0.3 cm. Here, the height  $h_t$ 

 $(h_r)$  refer to the distance between the phase center of Tx (Rx) horn and the bottom wall of the fabricated metal enclosure. Absorbers were used to eliminate the reflections from the backside of the antennas. Measured data was collected in the frequency band from 300 GHz to 312 GHz.

The measured path loss over the frequency band for different antenna heights,  $h = h_t = h_r$  are shown in Fig. 4b. As shown in the plot, there is an approximate 7 dB variation of the path loss with respect to the antenna heights which can be explained by the effects of the resonant modes inside the metal cavity. However, in comparison with the result of a similar measurement performed in a desktop size metal cavity shown in Fig.8 of [8], the path loss variation along the measured frequencies shown in Fig. 4b is limited to 4 dB which is much smaller than the 11 dB variation measured in the larger size cavity. This path loss variation can be illustrated with the concept of mode sensitivity. For a given frequency, the frequency sensitivity can be calculated as  $\Delta f/f = \lambda^3/(8\pi V)$ , where V is the volume of the cavity [9]. The  $\Delta f$  at 300 GHz is 2.56 and 19.71 KHz for the fabricated desktop size and Intel-mini size metal cavity, respectively. Larger value of  $\Delta f$  for the smaller cavity points to the less mode interference and consequently less path loss variation along the frequency. Since the cavity is symmetric, the measured mean path loss for the height of antennas, h varied from 0.3075 cm to 4.6925 cm can be estimated by flipping the measured results up and down. From the measurement, the standard deviation of shadowing factor,  $\delta$ , is determined to be 0.069 dB. By curve-fitting our path loss model with the interpolation of the measured path loss, it is found that the first fifteen TE modes dominate the resonant modes inside the Intel-mini size metal cavity. Also, the coefficients for each mode are estimated. Figure 4c compares the model prediction with the mean value of measured results at each height of the antennas. It can be observed from the figure that the model matches well with the measured results.

PDP represents the intensity of a signal received through a multipath channel as a function of time delay. The PDP of our proposed channel model can be calculated by taking the Inverse Fourier transform of the auto-correlation function of the wireless channel in the Intel-mini size metal cavity as  $p(\tau) = \mathcal{F}_{\Delta f}^{-1}\{R(\Delta f)\}$ . Figure 4d compares the simulated and measured PDP for the case  $h_t = h_r = 2.1075$  cm. It can be seen from the measured PDP that there are seven clusters of periodic later arriving peaks with the period of 0.73 ns. This periodic delay indicates that the extra distance covered by the later arriving signal is 22 cm which is twice of the cavity's length, which also implies that those periodic later arriving peaks are the results of the EM fields generated from the excited sidewalls of the cavity. To simplify the analysis, these periodic peaks can be treated as the results of MB rays which bounces back and forth between the two excited sidewalls. Comparing with PDP plot of the similar measurements performed in the desktop size metal cavity shown in Fig. 6d of [4], the periodic later arriving peaks measured in the smaller cavity have smaller amplitudes comparing with the amplitudes of the

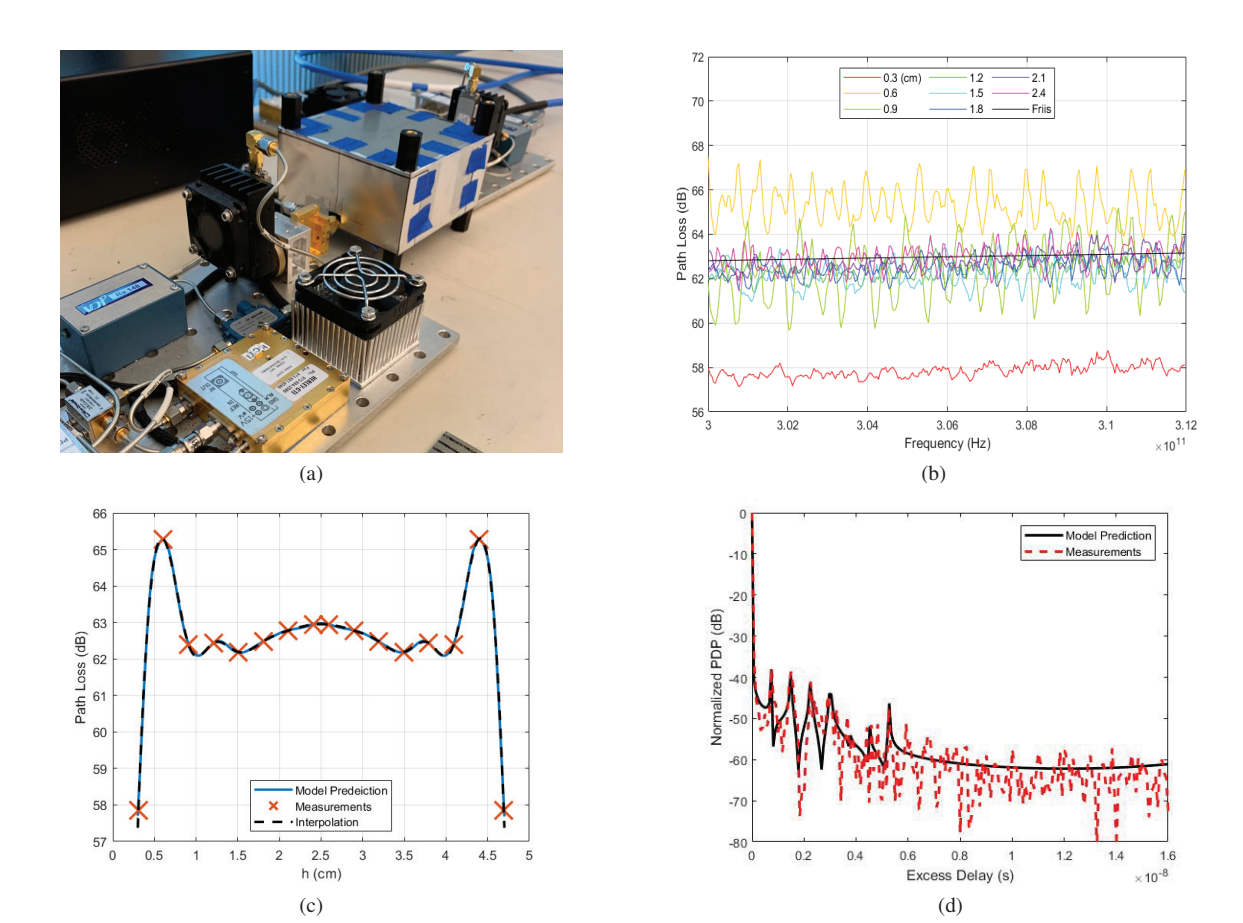


Fig. 4. LoS propagation in an Intel-mini size metal cavity at 300 GHz with  $h_t$  and  $h_r$  ranging from 0.3075 cm to 2.4075 cm: (a) Measurements setup, (b) Measured path loss over the frequency band, (c) Comparison of the theoretical and measured path loss with respect to h, and (d) Comparison of the normalized simulated and measured PDPs.

later arriving peaks measured in larger cavities. This can also be explained by the mode sensitivity. In the reference model, the Ricean factor K is estimated to be 27.28. For the MB component, the number of later arriving rays is chosen to be 7. Parameters  $k_1=0.065,\ k_2=0.165,\ k_3=0.2,\ k_4=0.25,\ k_5=0.01,\ k_6=0.05,\ \text{and}\ k_7=0.26.$  It can be observed from Fig. 4d that the simulated PDP matches well with the measured result in both amplitudes and the excess delay.

# V. CONCLUSIONS

In this paper, we presented a path loss model and a geometry-based statistical model for Terahertz (THz) chip-tochip wireless communication in nettop size metal enclosures based on our previous work in a desktop size metal enclosure. Besides the resonant-based power variation in the metal cavity and the loss due to the radiation pattern of antenna, the proposed path loss model also captures the attenuation of traveling wave and the gain of the electromagnetic horn in near region. The proposed geometric model describes the propagation of the traveling wave and the wave generated from the excited walls as a superposition of line of sight (LoS) and multi-bounced (MB) rays. From the geometrical model, the frequency correlation functions and the power delay profiles have been derived. Measurements for LoS propagation in near region have been performed in the indoor environment and in a nettop size empty metal enclosure. The measured results match

well with the model predictions, which verified the correctness of our model.

## REFERENCES

- S. Kim and A. Zajić, "Characterization of 300-GHz wireless channel on a computer motherboard," *IEEE Transactions on Antennas and Propaga*tion, vol. 64, no. 12, pp. 5411–5423, Dec 2016.
- [2] T. Kürner, A. Fricke, S. Rey, P. Le Bars, A. Mounir, and T. Kleine-Ostmann, "Measurements and modeling of basic propagation characteristics for intra-device communications at 60 GHz and 300 GHz," *Journal of Infrared, Millimeter, and Terahertz Waves*, vol. 36, no. 2, pp. 144–158, 2015.
- [3] J. Fu, P. Juyal, B. B. Yilmaz, and A. Zajić, "Investigation of resonance based propagation loss modeling for thz chip-to-chip wireless communications," in 2020 14th European Conference on Antennas and Propagation (EuCAP), 2020, pp. 1–5.
- [4] J. Fu, P. Juyal, and A. Zajić, "Modeling of 300 ghz chip-to-chip wireless channels in metal enclosures," *IEEE Transactions on Wireless Communications*, vol. 19, no. 5, pp. 3214–3227, 2020.
- [5] H. G. Schantz, "Near field propagation law a novel fundamental limit to antenna gain versus size," in 2005 IEEE Antennas and Propagation Society International Symposium, vol. 3A, 2005, pp. 237–240 vol. 3A.
- [6] T. S. Chu and R. A. Semplak, "Gain of electromagnetic horns," *The Bell System Technical Journal*, vol. 44, no. 3, pp. 527–537, 1965.
  [7] J. F. Johansson and N. D. Whyborn, "The diagonal horn as a sub-
- [7] J. F. Johansson and N. D. Whyborn, "The diagonal horn as a sub-millimeter wave antenna," *IEEE Transactions on Microwave Theory and Techniques*, vol. 40, no. 5, pp. 795–800, 1992.
   [8] J. Fu, P. Juyal, and A. Zajić, "THz channel characterization of chip-to-
- [8] J. Fu, P. Juyal, and A. Zajić, "THz channel characterization of chip-tochip communication in desktop size metal enclosure," *IEEE Transactions* on Antennas and Propagation, pp. 1–1, 2019.
- [9] P. Juyal, J. Fu, and A. Zajić, "Effect of modes on thz wireless channels inside metal enclosures," in 2020 33th General Assembly and Scientific Symposium (GASS) of the International Union of Radio Science (URSI), 2020, pp. 1–2.